Spatiotemporal Dynamics of the Landolt Reaction in an Open Spatial Reactor with Conical Geometry

Vincent Labrot, Anne Hochedez, Philippe Cluzeau, and Patrick De Kepper*

Centre de Recherche Paul Pascal, C.N.R.S., 115 Avenue Dr. A. Schweitzer, F-33600 Pessac, France

Received: July 25, 2006; In Final Form: October 11, 2006

In a previous study, the iodate−sulfite proton autoactivated reaction (Landolt reaction) was shown to exhibit spatial bistability and spatiotemporal oscillations when operated in an open spatial reactor with fixed "thickness", i.e., feed boundary to core distance. Here, we show that the spatial reactors with conical geometry enable one to rapidly probe the sensitivity of the above phenomena over a large range of the "thickness" parameter. This often-neglected parameter in chemical pattern studies plays an important role on the selection and stability of states. We reveal that the quenching capacity of slow diffusing polyacrylate ions on the spatiotemporal oscillations depends on this "thickness". The presented results should be useful for further research on reaction diffusion patterns and chemomechanical structures.

1. Introduction

Chemical patterns in reaction−diffusion systems are a paradigm for self-organization phenomena far from thermodynamic equilibrium.[1,2] The studies of these patterns have made considerable progress, in the past decade, with the development of open spatial reactors. The most popular such reactors consist of a thin piece (disk,[3−6] annular strip,[7] long cylinder[8]) of hydrogel diffusively fed by contact of one face with the contents of a continuous stirred reservoir of chemicals, one-side fed reactors (OSFR). In these and other feeding geometries, many different sustained spatiotemporal patterns such as excitability waves,[9] stationary Turing,[10−11] spatiotemporal intermittency,[12] and front patterns[4,13] could be observed and bifurcations between them could be finely studied.

It was gradually realized that the way reaction−diffusion patterns develop in real open spatial reactors is more involved than simple model approaches assume. In particular, fixed boundary composition (Dirichlet conditions) which leads to boundary layer effects has to be considered. These can play a key role in the existence and stability of states.[14] Partly because of these difficulties, the number of chemical systems which have been shown to develop sustained nontrivial patterns are still few. Beside the popular and well understood Belousov−Zhabotinsky (BZ) and chlorite−iodide families of reactions, only three others, not including biochemical reactions, were shown to produce sustained spatiotemporal patterns. These include the ferrocyanide−iodate−sulfite (FIS) reaction which has led to a wide variety of standing patterns.[15−17] However, there is no comprehensive understanding of the processes really at play in this system, yet. The presently studied reaction is a subpart of this reaction. More recently, the chlorite−tetrathionate (CT)[7,8,18] and iodate−sulfite (IS)[19] pH driven autocatalytic reactions have been shown to develop "spatial bistability" and sustained wave patterns. The latter reaction is the main subject of this report.

Spatial bistability is a generic property of autoactivated reactions operated in one-side-fed open spatial reactors. In such spatial reactors concentration profiles of input chemicals and products naturally develop orthogonally to the feed-surface. They result from a dynamical balance between the consumption/production of chemicals in the hydrogel and the diffusive exchanges of these at the boundary. Here, the thickness "*l*" of the spatial reactor, i.e., the distance from the feeding boundary to the deep core of the reactor, plays a role somewhat analogous to that of the residence time in a continuous stirred tank reactor (CSTR). Over a finite range of *l* values, which depend on chemical feed parameters, two different stable chemical concentration profiles can coexist across the depth of the reactor for the same fixed chemical composition at the feeding boundary. A comprehensive description of the spatial bistability phenomenon can be found in reference 14.

It was recently shown, both theoretically and experimentally, that new sources of dynamical instabilities can be generated if "*l*" is made to couple to the chemical composition in the core of the spatial reactor.[20,21] The first experimental demonstration of such "chemomechanically" induced patterns was made by operating the spatial bistable CT reaction in a long cylindrical pH-responsive gel that swells and deswells when the solution in the core of the gel reactor is respectively alkaline or acid.[8] Traveling contraction waves and more complex spatiotemporal patterns could be obtained in these gel reactors after an initial local perturbation. However, due to intrinsic limitations of the swelling/deswelling ratio of the pH-sensitive gels and to the extreme slowness of the initial stage of the CT reaction, the direct bifurcation to oscillatory shapes[20] could not be induced. To explore such spontaneous elementary chemomechanical bifurcation to pulsating structures, it is necessary to explore other reaction systems to find spatial bistability with appropriate dependence on the *l* value of an OSFR. The determination of the dependence of spatial bistability on *l* is tedious in uniform OSFRs since this parameter cannot be continuously varied like other control parameters such as the temperature or the concentration of input species.[14] It has been proposed that the use of OSFRs with conical shape gels could provide a fast and easy way to determine the range and sensitivity of spatial bistability on the distance *l*.[22]

The present report further highlights how to make the most from the use of such simple open spatial reactors, with a uniform ramp of *l* values. Advantages and complications are discussed.

The purpose of the present studies is 3-fold: (1) To improve our understanding of spatiotemporal instabilities previously

10.1021/jp064728z CCC: $33.50
Published on Web 12/06/2006

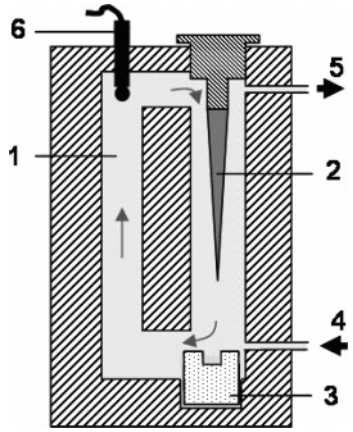

Figure 1. Schematic section of the open spatial reactor with a conical gel geometry. (1) Continuous stirred tank reactor (CSTR), arrows indicate gross recirculation of the vigorously stirred fluid; (2) conical piece of inert agarose gel; (3) magnetic stirring turbine; (4) inlet flow port for fresh reagents; (5) outlet flow port; (6) pH electrode.

observed in the iodate-sulfite (IS) reaction.[19] This includes the determination of the sensitivity of such dynamical instabilities on the geometric parameter *l*. (2) To make progress in our systematic search for symmetry breaking and standing reaction−diffusion patterns in different chemical systems.[13] This generally requires the development of short range activation processes. In the case of reactions where the main activation processes are driven by protons, the required short range activation can be induced by introducing large weight carboxylated species, such as polyacrylate ions. In the quest for sustained patterns, the parameter *l* of the OSFR can also play an important role, as seen in ref 16. (3) To find conditions, if any, for which the IS reaction could exhibit spatial bistability dependence over a range of *l* values narrower than the swelling/deswelling capacity of standard pH responsive gels.[23−25] Size changes in these gels rarely exceed a factor two as a function of pH.

2. Materials and Methods

The OSFRs used in the present experiments are thin truncated conical pieces of agarose gel (2% agarose from Fluka 05070). They were cast by filling yellow tips for micropipets from Poly Labo with a hot liquid solution of agarose. Cones of different sizes but with the same angle at the top were used. The ratio of the radius of the cones to the normal distance to virtual tip of the cone is 5%. The different conical OSFRs have the same small base radius of 0.25 mm but their large base and length differ. The longest conical gel has a large base radius R_{LB} = 2.25 mm and a distance between the large and small base of 40 mm. The two other smaller conical gels are obtained by cutting this distance approximately by half and by a quarter. The pieces of gel are carefully glued by their large base, with cyanoacrylate glue, on a plexiglass holder and suspended in a CSTR as sketched in Figure 1. The OSFR is fed with four precision pumps (Pharmacia P500). Two feed streams respectively contain fixed concentrations of potassium iodate (Aldrich, 99.5%), $[KIO_3] = 0.054$ mol·dm^{-3}, and sodium sulfite (Aldrich, 98%) $Na_2SO_3 = 0.18$ mol·dm^{-3} kept under nitrogen atmosphere. The iodate solution also contains 0.1 g·dm^{-3} of methyl orange (Aldrich), a pH color indicator that changes from yellow (basic) to red (acid) around pH = 3.7. Two others streams contain water and sulfuric acid ($[H_2SO_4] = 0.05$ mol·dm^{-3}) to control the pH of the input solution. Through these last streams, at a certain point in the experiments, controlled amounts of sodium poly(acrylate) (PA) (Polyscience, 20 000 Da) are also added to reduce the effective diffusivity of protons in the gel. The sum of all the input flows is kept constant and equal to 360 cm^{-3}/h which corresponds to a residence time $\tau = 7.1$ min. The sum of the iodate and sulfite solutions, and water and sulfuric acid solutions, was respectively kept constant at 240 cm^{-3}/h and 120 cm^{-3}/h. The iodate to sulfite feed ratio was changed by changing the relative flow of these solutions. The acid feed concentration is changed by changing the water to acid solution flows. The CSTR is thermostated at 30 °C. The state of the contents of the CSTR is monitored by a pH electrode. A CCD color camera connected to a time lapse VCR and to a frame grabber allows the monitoring of the state patterns in the gel.

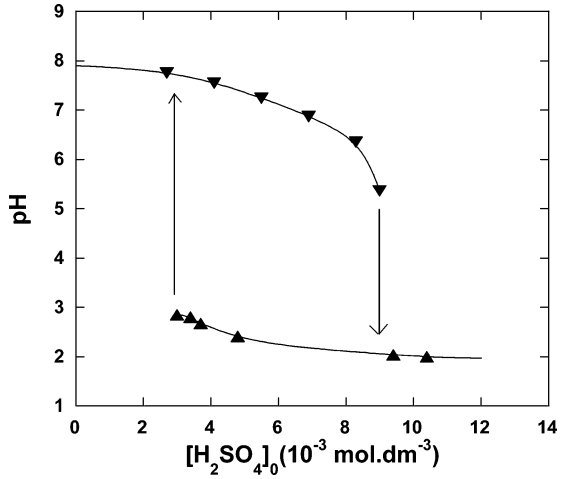

Figure 2. Bistability in the CSTR. Experimental conditions: $[IO_3^-]_0 = 0.018$ mol·dm^{-3}, $[SO_3^{2-}]_0 = 0.06$ mol·dm^{-3}. The symbols correspond to the experimental points and are attributed to the state of the CSTR: ▼ stable F state; ▲ stable T state; arrows indicate the values at which the switches from one branch to the other are observed.

3. Results

3.1. Batch and CSTR Dynamics. Let us recall some properties of the iodate−sulfite reaction. The reaction is autocatalytic both for protons and iodide ions.[26] The dominant process is the autocatalytic oxidation of hydrogen sulfite,

$$IO_3^- + 3HSO_3^- \rightarrow I^- + 3SO_4^{2-} + 3H^+ \qquad (1)$$

followed by the Dushman reaction in excess iodate:

$$IO_3^- + 5I^- + 6H^+ \rightarrow 3I_2 + 3H_2O \qquad (2)$$

Note that while the reaction (eq 1) is a proton-producing step in which the rate increases with increasing $[H^+]$,[27] eq 2 is a proton-consuming process.

In batch conditions, the dynamics of the IS reaction depends on the initial iodate/sulfite ratio. In an excess of sulfite ions ($[IO_3^-]_0/[SO_3^{2-}]_0 \leq 1/3$), the main products of the reduction of iodate ions are iodide and sulfate ions due to reaction 1. For the reactant concentrations used in this report, the pH drops from 7 to 2.5, after an induction time of 15−40 min. On the other hand, at $[IO_3^-]_0/[SO_3^{2-}]_0 \geq 1/3$ (excess of iodate ions), the end-products are iodine, triiodide, and sulfate ions. In this case the pH drops down similarly from 7 to about 2.5 (mainly due to eq 1) but then increases back to values up to 5.5, due to the subsequent reaction of iodide with the excess iodate (eq 2).

When the reaction is operated in a CSTR, bistability is readily observed as a function of $[H_2SO_4]_0$, the acid concentration in the total premixed feed flow (Figure 2). Note that sulfuric acid

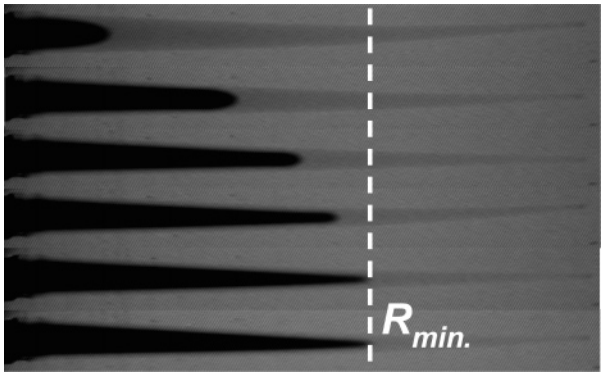

Figure 3. Snapshots of the cone of gel during the propagation and interface stabilization of the mixed state. Experimental conditions: $[IO_3^-]_0/[SO_3^{2-}]_0 = 0.35$, $[H_2SO_4]_0 = 4.86 \times 10^{-3}$ mol·dm^{-3}. From top to bottom, snapshots were respectively taking at 1, 7, 13, 22, 36, 45 min after the emergence of the acid core. Dark gray corresponds to the acid state of the color pH indicator. For other information, see text.

is used as control parameter because of its strong influence on the reaction kinetics. The competition between the time scale over which the reaction evolves and the input flow rate leads to bistability between a high pH branch (pH ≈ 8 to 5) referred to as the "F" branch corresponding to a branch of low extent of reaction, and a low pH branch (pH ≈ 3 to 2.5) referred to as the "T" branch, a branch of high extent of reaction. The stability of these two states can overlap over a range of control parameters. When the contents of the reactor is initially in the alkaline state at low $[H_2SO_4]_0$ and this control parameter is increased, the chemical state of the reactor follows the F branch until $[H_2SO_4]_0 = 8.9 \times 10^{-3}$ mol·dm^{-3}. Beyond this value, the system switches to the acid state branch T. If the $[H_2SO_4]_0$ value is then decreased, the chemical state of the reactor follows the T branch until $[H_2SO_4]_0 = 3 \times 10^{-3}$ mol·dm^{-3}, and at this value the system turns back to the F branch.

3.2. Spatial Reactor Dynamics. *3.2.1. Phase Diagram Constructions.* During all the spatial reactor observations, the contents of the CSTR is maintained on the high pH branch. In this condition, previous studies in an annular OSFR with an uniform value of l show that bistability can be observed. In one state the gel contents are uniformly filled with an "unreacted" composition also referred to as the F state, while the other state exhibits a sharp transition from an unreacted composition next to the feed boundary to a reacted composition in the core. This state is referred to as the mixed state or M state.[19] The F state is uniformly pale yellow while the M state is characterized by a sharp color switch from yellow at the boundary to dark red in the core. The observations made with conical gels having different R_{LB} values are gathered in (R, $[H_2SO_4]_0$) planes. The different cones are immersed in the CSTR contents one after the other. Starting with a low value of $[H_2SO_4]_0$, this parameter is increased stepwise. The feeds are maintained fixed for at least 2h after each change of parameter value. Initially, the cones are in the uniform clear yellow F state. After a critical step of increasing $[H_2SO_4]_0$, the large base of the cones spontaneously turns red indicating that at this R_{LB} value, the F state is no longer stable and a transition to the M state is observed (Figure 3). In the (R, $[H_2SO_4]_0$) diagrams (Figures 4 and 5), the symbol ● marks the middle of this supercritical increment of parameter value, and the associated "error bar" corresponds to the actual size of the step. The R_{LB} curve sets the upper limit for the observation of cones uniformly in the F state. After the M state has spontaneously appeared, it invades smaller sections of the conical gel, as illustrated in Figure 3. This propagation stops at a minimal radius value marked by the symbol ■. This stable F/M interface sensitively depends on $[H_2SO_4]_0$. It respectively moves to smaller or larger radius when $[H_2SO_4]_0$ is increased or decreased. Within our experimental accuracy, the radius at which this interface stabilized does not depend on the cone length. Curve R_{min} marks this limit. Naturally, the critical parameter value at which the M state spontaneously appears depends on the value of R_{LB}.

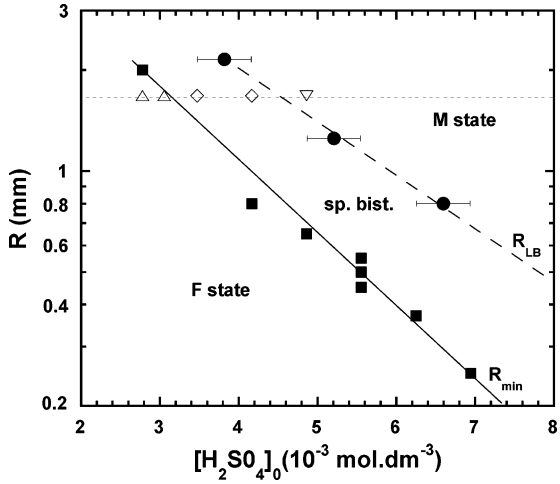

Figure 4. Diagram in the (R, $[H_2SO_4]_0$) plane. Experimental conditions: $[IO_3^-]_0 = 0.020$ mol·dm^{-3}, $[SO_3^{2-}]_0 = 0.055$ mol·dm^{-3} ($[IO_3^-]_0/[SO_3^{2-}]_0 = 0.35$). The symbols ● and ■ correspond, respectively, to the experimentally observed spontaneous appearance and limit of propagation of a stable mixed state. The dash (R_{LB}) and full (R_{min}) curves are the respective limits of steady-state bistable states compositions in the conical OSFR. Open symbols correspond to different states observed in a cylindrical gel (radius $R = 1.65$ mm): △ monostable F state, ◇ spatially bistable state, ▽ monostable M state.

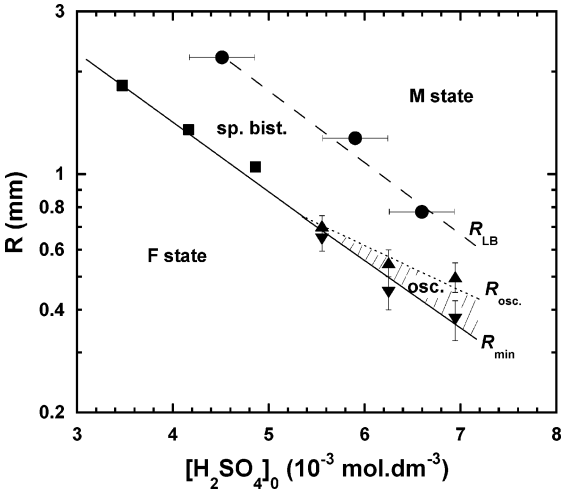

Figure 5. Diagram in the (R, $[H_2SO_4]_0$) plane at $[IO_3^-]_0/[SO_3^{2-}]_0 = 0.32$. The symbols (■, ●) and the dash and full curves have the same meaning as in Figure 4. The hatched region corresponds to the space amplitude of oscillations of the acid composition in the core of the conical OSFR. The symbols ▲ and ▼ delimit the experimentally observed starting and stopping position of associated acid waves. Vertical error bars indicate the uncertainties on determination of these positions. The dotted curve (R_{osc}) corresponds to the limit between a stable and oscillatory acid core state.

3.2.2. Effect of Iodate/Sulfite Ratio. Experiments were performed at three different fixed $[IO_3^-]_0/[SO_3^{2-}]_0$ ratios corresponding to three characteristic sections in the cross shape phase diagram previously established[19] in an annular OSFR with a fixed value of $l = 1$ mm.

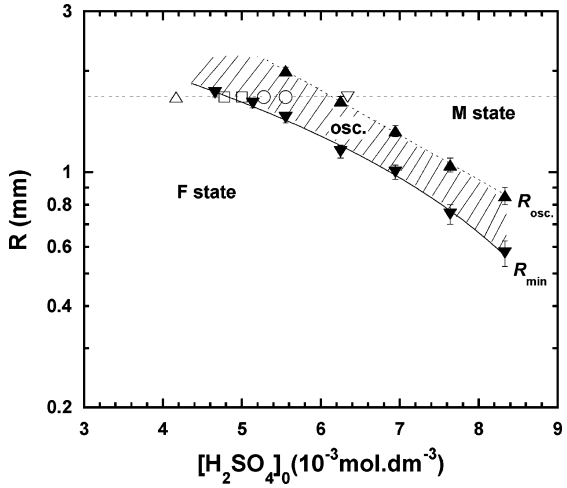

Figure 6. Diagram in the (R, $[H_2SO_4]_0$) plane at $[IO_3^-]_0/[SO_3^{2-}]_0 = 0.30$. The symbols and curves have the same meaning as in Figure 5. Open symbols correspond to the different states observed in a cylindrical gel ($R = 1.65$ mm): △ monostable F state, □ excitable state, ○ oscillatory state, ▽ monostable M state; for more details, see text.

• The diagram in Figure 4 was established at a $[IO_3^-]_0/[SO_3^{2-}]_0$ value fixed at 0.35. This ratio value corresponds to a slight excess of iodate. The experiments are made in cones with three different R_{LB} values. In all cases, at low values of the acid feed, the whole cone is in the uniform clear color F state and remains in this state until a supercritical change in $[H_2SO_4]_0$ is reached. In the figure, the dashed (R_{LB}) and full (R_{min}) curves delineate respectively the value at which the F state loses stability in a cone with a large base R_{LB} and the minimum radius at which the M state can be observed at fixed acid feed. According to the history of the system, the top part of the cone may be either in the M state or in the F state. Between these two limits, the top part of the cone presents bistability between the stable F and M states. Note that the R_{LB}/R_{min} ratio range from 1.8 to 2.9 when $[H_2SO_4]_0$ changes from 3.8×10^{-3} to 7×10^{-3} mol·dm^{-3}.

• At $[IO_3^-]_0/[SO_3^{2-}]_0 = 0.32$, a value close to the stoichiometric ratio of eq 1, Figure 5 gathers the results also obtained in cones with three different R_{LB} values. The critical stability limit of the F state at R_{LB} does not differ much from that in Figure 4. When a part of the cone is in the M state, this part stabilizes at a fixed R_{min} position at low $[H_2SO_4]_0$. However, for $[H_2SO_4]_0 \geq 5.1 \times 10^{-3}$ mol·dm^{-3} the R_{min} value becomes unstable and oscillates periodically between two generally fixed positions R_{osc} and R_{min} as indicated in diagram Figure 5. The oscillations appear as periodic traveling acid waves which, in the core of the cone start at R_{osc}, and die at R_{min}. Note that the relative space amplitudes of these oscillations increase with increasing $[H_2SO_4]_0$. In this case, the upper part of the cones, for $R_{LB} \geq 1.3$ mm, exhibits bistability between stable F and M states, similar to the previous case. For cones with $R_{LB} < 1.3$ mm, bistability occurs between an F state and, a stable M state for $R > R_{osc}$ or an oscillatory state for $R_{min} < R < R_{osc}$.

• Figure 6 presents the observations made when $[IO_3^-]_0/[SO_3^{2-}]_0 = 0.30$, a value corresponding to a slight excess of sulfite. Contrary to the previous cases, the results gathered in this figure correspond to cones with the same large base $R_{LB} = 2.25$ mm. As usual, at low $[H_2SO_4]_0$ and up to $[H_2SO_4]_0 = 5.1 \times 10^{-3}$ mol·dm^{-3} the whole cone is in the F state. An increase to $[H_2SO_4]_0 = 5.5 \times 10^{-3}$ mol·dm^{-3} induces the spontaneous development of the M state at R_{LB}. As usual this acid core state propagates down to lower radius. However, the M state does not stabilize at a fixed position but immediately oscillates. Along the central axis of the cone, periodic acid wave trains that start at R_{osc} and die at R_{min} are observed (Figure 7). If $[H_2SO_4]_0$ is then decreased back to 5.1×10^{-3} mol·dm^{-3}, the cone returns to the F state without hysteresis. Note that R_{min} values for $[H_2SO_4]_0 < 5.5 \times 10^{-3}$ mol·dm^{-3} were obtained by triggering a wave with a small acid perturbation at the large base of the cone. On the contrary, if the $[H_2SO_4]_0$ value is increased, the oscillatory part of the cone progressively shifts toward smaller radius. As shown in the log−log plot in Figure 8 the period of the wave trains follows a power law as a function of R_{osc}. From the slope of the best fit straight curve we obtain a value of 1.9 ± 0.2. A value consistent with the power 2 value expected for a purely diffusive process.

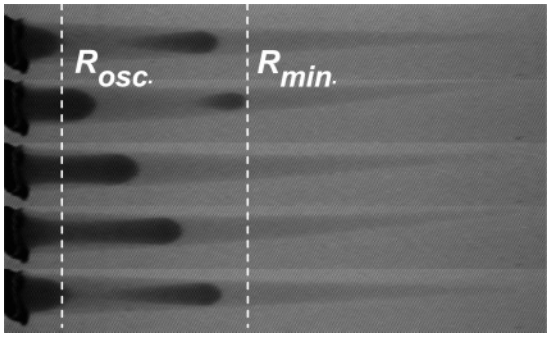

Figure 7. Sequences of snapshots illustrating the periodic acid waves observed in the cone. Interval of time between each snapshot is of 5 min. Time increases from top to bottom. Experimental conditions: $[IO_3^-]_0/[SO_3^{2-}]_0 = 0.30$, $[H_2SO_4]_0 = 5.55 \times 10^{-3}$ mol·dm^{-3}.

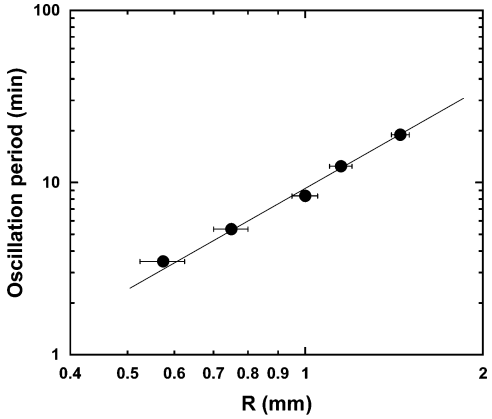

Figure 8. Oscillation period of the wave-trains as a function of R_{osc}. Log−Log plot; horizontal bars account for the experimental uncertainties on R_{osc}.

3.3. Effect of PAA Concentration on the Dynamics. It is known that the introduction of large molecular weight carboxylated species in this reaction−diffusion system quenches oscillatory and excitability phenomena.[19] This is due to the reduction of both the effective reactivity and effective diffusivity of protons. Here we report more refined studies on the quenching of spatiotemporal instabilities by introducing polyacrylate (PA) ions in the feed solutions and in the gel.

We focus on the case where the $[IO_3^-]_0/[SO_3^{2-}]_0 = 0.30$, that is when oscillatory behaviors can be observed at all values of R (Figure 6). The addition of PA affects the steady-state bistability range of the CSTR. The result is displayed in Figure 9 for $[PA]_0 = 1 \times 10^{-3}$ mol·dm^{-3} (concentration in carboxylate units). The bistability domain is globally shifted to higher values of $[H_2SO_4]_0$ due to the partial protonation of carboxylate functions and the associated pH buffering effect.

We tested the stability of spatial states in conical OSFRs with three different R_{LB} values. The results are displayed in Figure

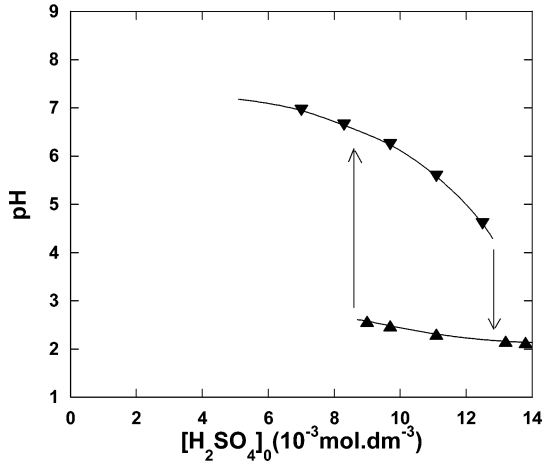

Figure 9. Bistability in the CSTR in presence of PA ($[PA]_0 = 0.01$ mol·dm^{-3}). Other experimental conditions and the meaning of the symbols are the same as in Figure 2.

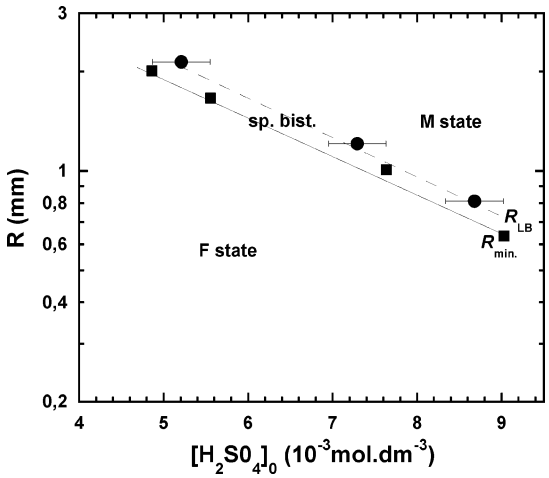

Figure 10. Diagram in the (R, $[H_2SO_4]_0$) plane at $[IO_3^-]_0/[SO_3^{2-}]_0 = 0.30$ and $[PA]_0 = 0.01$ mol·dm^{-3}. The symbols and the curves have the same meaning as in Figure 4.

10. Note that at this value of $[PA]_0$, oscillations are totally quenched and are replaced by a narrow domain of spatial bistability at all values of R. In these feed conditions, the R_{LB}/R_{min} ratio drops to 1.15 ± 0.05. Interestingly, this spatial bistability domain falls exactly in the $[H_2SO_4]_0$ and R_{LB} domain values at which oscillations were observed in the absence of PA. Though the CSTR bistability is shifted to higher $[H_2SO_4]_0$ values, the spatial bistability location is grossly invariant.

Similar studies were made at intermediate values of $[PA]_0$. At $[PA]_0 = 1 \times 10^{-3}$ mol·dm^{-3}, there is no qualitative difference with what is observed in the absence of PA. At $[PA]_0 = 3 \times 10^{-3}$ mol·dm^{-3}, oscillations are only partly quenched. The observations made in a cone with $R_{LB} = 2.25$ are presented in Figure 11. At low values of $[H_2SO_4]_0$ the F/M interface is stable but when on increasing $[H_2SO_4]_0$ the interface drops below a critical R_{min} value, its position becomes oscillatory just as observed in the diagram in Figure 5. This is a remarkable observation showing that the critical PA value for quenching oscillatory instabilities can be sensitive on the l value of the OSFR, e.g., here the value of R.

4. Discussion

One of the interests of working on systems with a ramp of parameter, e.g., the distance from the feed surface to the core of an OSFR, is to be able to extrapolate the local information,

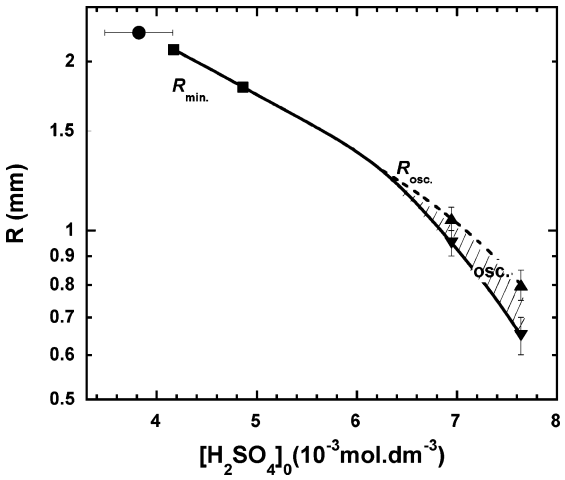

Figure 11. Position of the M state interface in the (R, $[H_2SO_4]_0$) plane at $[IO_3^-]_0/[SO_3^{2-}]_0 = 0.30$ and $[PA]_0 = 3 \times 10^{-3}$ mol·dm^{-3}. Symbols and curves have the same meaning as in Figure 5.

on state selection and stability along the ramp, to the case of uniform environment. This is not a trivial problem in reaction−diffusion systems where nonpotential effects and multistability phenomena are at play. The diagrams in Figures 4, 5, 6, and 10 are no standard phase diagrams in the R and $[H_2SO_4]_0$ phase space. If the R_{LB} curves correspond to the stability limit of the states in the (R, $[H_2SO_4]_0$) constraint space; the radius R_{min} down to which the M state extends is not directly controlled by the observer but is a response of the system to the initial conditions and the imposed $[H_2SO_4]_0$ value. Nevertheless, we infer that the R_{min} curves are good approximations of the stability limit of the M state at this value of R in a system with constant radius.

To test this statement, we have replaced the cone by a cylindrical gel of radius $R = 1.65$ mm in the feed conditions of Figure 4. As previously, the cylinder of gel is initially set in the F state when $[H_2SO_4]_0$ is low. This control parameter is then increased until a critical value corresponding to the spontaneous switch of the gel in the mixed state (circle symbol in the phase diagrams). Within the $[H_2SO_4]_0$ incremental steps, this transition corresponds to the limit of stability of the F state established with the cone. When $[H_2SO_4]_0$ is then decreased, the gel contents follow a hysteretic behavior. It stays in the mixed state until another, lower critical value is reached, where it switches back to the flow state. This transition fits very well with the R_{min} value interpolated from the experiments in the cones. The R_{min} corresponds to the isostability point of an interface between the M and F state and not to the stability limit of the M state. However, it is commonly observed in chemical systems that this neutral stability point of an interface between two steady states is strongly shifted to the stability limit of the state with the largest extent of reaction.[21,27,28]

Analogous experiments were developed when $[IO_3^-]_0/[SO_3^{2-}]_0 = 0.30$ (Figure 6), that is when oscillations can be observed at all values of R in the cone. The $R = 1.65$ mm cylindrical gel, initially in the F state at low $[H_2SO_4]_0$, stays in this uniform color state up to 5.0×10^{-3} mol·dm^{-3} and switches to an oscillatory M state at 5.3×10^{-3} mol·dm^{-3} and 5.6×10^{-3} mol·dm^{-3} (see open symbols in Figure 6). Oscillations appear as uniform pulsations of the radial extension of the acid state in the core of the cylinder. At 6.2×10^{-3} mol·dm^{-3} the cylinder is in a stable M state. If changes in $[H_2SO_4]_0$ are reversed, the oscillatory behavior resumes and vanishes at the same step values. In the vicinity of the oscillatory M state, the F state of the gel was found to be excitable. When an acid perturbation is made at one end of the cylinder, an undamped

acid pulse propagates along the axis. See corresponding open symbols in Figure 6. This figure shows that the accumulative domains of oscillatory and excitable behavior in the cylinder nearly quantitatively follow the parameter window for which oscillatory behavior is observed in the cone at R = 1.65 mm. In the cone, self-oscillatory and excitability domains cannot be distinguished except at the R_{LB} value of the cone, as explained for the determination of the R_{min} values for $[H_2SO_4]_0$ lower than the value at which an acid core spontaneously appears.

Aside from the study of the role played by $l \equiv R$ on the existence and stability of states as a function of major reactants, we show that the quenching of the oscillatory spatiotemporal behavior by introducing polyacrylate into the system also depends on the size parameter *l*. The introduction of such an acid buffering species both reduces the apparent reactivity and diffusivity of the protons. Szalai & De Kepper[19] had previously shown that the introduction of such carboxylated species quenches oscillations. In this previous work, it was gathered that the oscillatory reaction−diffusion instability observed in the IS reaction mainly originates from the faster diffusion of the activator, i.e., the proton, compared to that of the major feed reagents. The present observation that the oscillatory behavior is longer lived at a small radius than at a large one when PA is introduced challenges this initial proposition. The shorter the radius the less the time scale separation between dynamics of the activator and of the feed species can develop through differential diffusion. Small values of *R* should not favor oscillations induced by differential diffusion. The smaller the *R* the more the chemical composition in the gel should be similar to that of the homogeneous composition of the CSTR. In the chlorite−tetrathionate pH autoactivated reaction, it is shown both theoretically and experimentally that differential diffusion oscillatory instabilities are favored by an increase of *l*.[7] The contrary observation with the IS reaction could infer that the oscillatory behaviors mainly originate from an homogeneous kinetic instability. However, to our knowledge, no CSTR oscillations were observed so far with the IS reaction. It is also noteworthy that numerical OSFR simulation of the IS reaction using the simplified kinetic mechanism proposed by Rabai and co-workers,[27] which accounts well for the observed CSTR dynamics and for the spatial bistability phenomena, does not reproduce spatiotemporal oscillation seen in experiments for any reasonable set of diffusion coefficients of species.[29] The kinetic and/or diffusional mechanisms of the IS reaction are more involved than usually inferred.

One of the objectives of this work was to find experimental conditions for which size changes of standard pH-sensitive gels would be able to spontaneously cross the low and high *l* bistability limits of the acid (M) and the alkaline (F) spatial states to produce self-sustained chemomechanical oscillations. This implies that the R_{LB}/R_{min} ratio be smaller than the corresponding radius ratio of the swollen and deswollen states of the pH-responsive gels. Let us recall that the shrinking between an alkaline and an acidic medium of a standard pH-responsive gel does not exceed a factor of 2, in ionic solutions typical for our present bistable system. At $[IO_3^-]_0/[SO_3^{2-}]_0 = 0.35$, the values of the R_{LB}/R_{min} ratios that can be drawn from the phase diagram (Figure 4) show that the size changes necessary to reach the respective high and low stability limits of the swollen F and shrunken M states, at fixed $[H_2SO_4]_0$, would be difficult or impossible to fulfilled. The critical size ratio decreases with decreasing value of $[IO_3^-]_0/[SO_3^{2-}]_0$. However, at $[IO_3^-]_0/[SO_3^{2-}]_0 \leq 0.32$, spatiotemporal oscillatory instabilities develop in the absence of chemomechanical feed back. Under these conditions the onset of chemomechanical instabilities would be difficult to demonstrate. Fortunately, the introduction of acrylate functions into the system quenches the oscillatory reaction−diffusion instability. Standard pH-responsive gels incorporate such functions in the network at typical concentrations of 10^{-2} mol·dm^{-3}. A concentration of the same order of magnitude than the one used in the phase diagram in Figure 10 for which the R_{LB}/R_{min} ratio has dropped as low as 1.15. The IS reaction thus provides spatial bistability properties suitable for further exploration of chemomechanical instabilities.

5. Conclusion

Though the observations in conical OSFR has to be carefully analyzed, like in all systems with a parameter ramp, we show that it is an easy and convenient way to analyze the effect of feed surface to core distance on the stability of states. We have been able to determine with a satisfactory accuracy the monostability, bistability, and oscillatory plus excitability limits over a wide range of size and other feed parameters in a minimal number of experiments. The present work further shows that the mechanisms at the origin of the oscillatory and excitatory reaction−diffusion patterns observed in this reaction are quite involved. Contrary to the case of the chlorite−tetrathionate reaction where the CSTR and the OSFR dynamics could be quasiquantitatively accounted by an overall kinetic equation plus some rapid acid equilibriums, in the present case, a more comprehensive kinetic and diffusional model is required.

Acknowledgment. This research has been supported by an ANR grant. We thank J. Boissonade and I. Szalai for stimulating discussions.

References and Notes

(1) Kapral, R.; Showalter, K., Eds. *Chemical Patterns and Waves*; Kluwer Academic Publisher: Amtersdam, 1995.
(2) Epstein, I. R.; Pojman, J. *An Introduction to Nonlinear Chemical Dynamics*; Oxford University Press: New York, 1988.
(3) Skinner, G. S.; Swinney, H. L. *Phys. D* **1991**, *48*, 1.
(4) Lee, K. J.; McCormick, W. D.; Ouyang, Q.; Swinney, H. L. *Science* **1993**, *261*, 192.
(5) Davies, P. W.; Blanchedeau, P.; Dulos, E.; De Kepper, P. *J. Phys. Chem. A* **1998**, *102*, 8236.
(6) Rudovics, B.; Barillot, E.; Davies, P. W.; Dulos, E.; Boissonade, J.; De Kepper, P. *J. Phys. Chem. A* **1999**, *103*, 1790.
(7) Boissonade, J.; Dulos, E.; Gauffre, F.; Kuperman, M.; De Kepper, P. *Faraday Discuss.* **2001**, *120*, 353. Fuentes, M.; Kuperman, M. N.; Boissonade, J.; Dulos, E.; Gauffre, F.; De Kepper, P. *Phys. Rev. E* **2002**, *66*, 56205.
(8) Labrot, V.; De Kepper, P.; Boissonade, J.; Szalai, I.; Gauffre, F. *J. Phys. Chem. B* **2005**, *109*, 21476.
(9) Noszticzius, Z.; Horsthemke, W.; Mc Cormick, W. D.; Swinney, H. L.; Tam, W. Y. *Nature* **1987**, *329*, 619. Dulos, E.; Boissonade, J.; De Kepper, P. *Phys. A* **1992**, *188*, 120.
(10) Castets, V.; Dulos, E.; Boissonade, J.; De Kepper, P. *Phys. Rev. Lett.* **1990**, *64*, 2953. Rudovics, B.; Dulos, E.; De Kepper, P. *Phys. Scr.* **1996**, *T67*, 43.
(11) Ouyang, Q.; Swinney, H. L. *Nature* **1991**, *352*, 610. Ouyang, Q.; Gunaratne, G. H.; Swinney, H. L. *Chaos* **1993**, *3*, 707.
(12) Perraud, J. J.; De Wit, A.; Dulos, E.; De Kepper, P.; Dewel, G.; Borkmans, P. *Phys. Rev. Letter* **1993**, *71*, 1272. De Kepper, P.; Perraud, J. J.; Rudovics, B.; Dulos, E. *Int. J. Bifurcation Chaos Appl. Sci. Eng.* **1994**, *4*, 1215.
(13) Szalai, I.; De Kepper, P. *J. Phys. Chem.* **2004**, *108*, 5315.
(14) Blanchedeau, P.; Boissonade, J.; De Kepper, P. *Phys. D* **2000**, *147*, 283.
(15) Lee, K. J.; Swinney, H. *Phys. Rev. E* **1995**, *51*, 1899.
(16) Li, G.; Ouyang, Q.; Swinney, H. L. *J. Chem. Phys.* **1996**, *105*, 10830.
(17) Lee, K.-J.; Mccormick, W. D.; Pearson, J. E.; Swinney, H. L. *Nature* **1994**, *369*, 215.
(18) Szalai, I.; Gauffre, F.; Labrot, V.; Boissonade, J.; De Kepper, P. *J. Phys. Chem. A* **2005**, *109*, 7843.
(19) Szalai, I.; De Kepper, P. *Phys. Chem. Chem. Phys.* **2006**, *8*, 1105.

(20) Boissonade, J. *Phys. Rev. Lett.* **2003**, *90*, 188 302.
(21) Strier, D.; Boissonade, J. *Phys. Rev. E* **2004**, *70*, 016210.
(22) Gauffre, F.; Labrot, V.; Boissonade, J.; De Kepper, P.; Dulos, E. *J. Phys. Chem. A* **2003**, *107*, 4452.
(23) Tanaka, T.; Fillmore, D.; Sun, S.-T.; Nishio, I.; Swislow, G.; Shak, A. *Phys. Rev. Lett.* **1980**, *45*, 1636.
(24) Huglin, M.; Liu, Y.; Velada, J. *Polymer* **1997**, *38*, 5785.
(25) Motonaga, T.; Shibayama, M. *Polymer* **2001**, *42*, 8925.
(26) Landolt, H. *Ber. Dtsch. Chem. Ges.* **1886**, *19*, 1316.
(27) Rábai, G.; Kaminaga, A.; Hanazaki, I. *J. Phys. Chem.* **1995**, *99*, 9795.
(28) Blanchedeau, P.; Boissonade, J. *J. Phys. Rev. Lett.* **1998**, *81*, 5007.
(29) Boissonade, J. Unpublished work.